J A S T
Journal of Aerospace Science and Technology

Effect of Wing Sweep Angle on The Vortex Interaction of a Tail-Wing Configuration

I. Bahman-Jahromi[1], M.R. Soltani[2], and M. Masdari[3]

The goal of this investigation is to study the effect of wing sweep angle on horizontal wing-body- tail configurations in subsonic flow. For this purpose, a series of wind tunnel tests were conducted on a model having a moveable horizontal tail and a wing planform with different sweep angles. Tests were performed at different tail deflection angles. Static surface pressure distribution over the suction side of wing was measured for both static and dynamic changes of the tail angles of attack. The strength of the vortices over different wings was compared and the effect of tail deflection on the wing flow field was investigated. It is seen that the wing sweep angle is a dominant factor for the strength of the vortices over the wing and hence the maneuverability of the vehicle.

Keywords: *Tail, Delta Wing, Vortex, Wind Tunnel*

Nomenclature

V_∞	Freestream Velocity (m/sec)
C_p	Pressure Coefficient $= \dfrac{(P - P_\infty)}{q_\infty}$
P_∞	Wind Tunnel Static Pressure
q_∞	Dynamic Pressure $= (1/2 \, \rho_\infty V_\infty^2 (N/m^2)$
ρ_∞	Air Density (Kg/m^3)
Re	Reynolds Number $= \dfrac{\rho_\infty V_\infty C}{\mu}$
C	Wing Root Chord (cm)
b	Wing Span (cm)
α_t	Tail Angle of Attack (*Deg.*)
α_w	Wing Angle of Attack *(Deg.)*
$\Delta\alpha$	Tail Deflection Angle $= \alpha_t - \alpha_w$ *(Deg.)*
Λ_w	Wing Sweep Angle
AR	Wing Aspect Ratio

Abbreviation

AOA	Angle of Attack (*Deg.*)
LE	Leading Edge
PSD	Power Spectrum Density

1. (Corresponding Author), Ph.D. Student, Dep't. of Aerospace Eng., Sharif University of Technology, Tehran, Iran. Email address: imanbahman@alum.sharif.edu
2. Professor, Dep't. of Aerospace Eng., Sharif University of Technology, Tehran, Iran. Email address: msoltani@sharif.edu
3. Assistant Prof., Univ. of Tehran.

1 Introduction

Control surfaces are used in combat aircraft to control the pitching moment and to help the vehicle perform high angle of attack maneuvers. For delta wing configuration, the flow characteristics around the horizontal tail depend on the wing and tail flow field and on their interactions. The flow over delta wing is mainly characterized by strong vortices. These vortices move downstream and affect the tail flow field making the problem more complicated. Many researches have been performed aimed at developing a practical method for shape optimization of the vehicle equipped with these types of wings [1-3]. In the next section, some information is presented to describe the importance and difficulties of predicting and designing efficient control surfaces.

The most efficient means to control projectiles and, hence, guide them to the desired target is through controlling their fins. The maneuvering force is generated in two different ways for aerodynamically controlled projectiles: rotation of the projectile to higher alpha as in tail or canard controlled projectiles, or by direct action near the center of gravity as in the mid-wing controlled projectiles [4].

Tail is the most useful control surface for long range projectiles. This control surface increases maneuverability of the projectile significantly. In addition, its almost linear aerodynamic interferences is another factor that makes its usage in the tail control projectiles more attractive. Usually a constant wing is added to these projectiles to gain a better lifting force [4].

Even though CFD is used to find the optimal fin shape and aerodynamic characteristics of the projectile, this method can be expensive and time consuming even after the exponential growth in the computational power nowadays. To avoid this dilemma, there are few engineering codes that can predict the aerodynamic characteristics of various configurations operating at different angles of attack and Mach numbers. All of these codes are based on the wind tunnel tests.

An example of using Experimental data to validate the predicted data is presented in Ref. [5]. Experimental data for a wing-body-tail configuration has been reported By Blair [6]. A few aerodynamic coefficients are estimated using a prediction code for a free stream Mach number of 1.7 and for a range of angle of attack from -2 to +18 deg. Comparison between the estimated and experimental data is presented in Ref. [5].

Roshanian presents some formulations for the multidisciplinary design optimization (MDO) [7]. Engineering codes have been validated for A.O.As up to 90⁰ for different configurations [8]. Several Experimental data are available for canard controlled models for both fixed and rolling tail fins [9]. Engineering codes have also been validated with these experimental data. Dahalan [10] presents user friendly and in-house software which is able to estimate the aerodynamic coefficients for different wing, body, wing-body, and wing-body-tail combinations.

Tests indicate nonlinearities associated with the vortex interactions between fin sets and body. To have a good prediction code, one must be familiar with physics of the vertical flow interactions between all parts of the projectile. One of the most complex configurations is wing-body-tail configuration. To author's knowledge, most of the present engineering codes are not still capable of an accurate prediction of the aerodynamic coefficients of this complex configuration especially at moderate to high angles.

In this research, a configuration including body, wing and tail was tested in a subsonic wind tunnel. Variations of the surface pressure distribution on the wing with effects of upwash caused by different tail deflections were tested for wings with sweep angles of 30 and 60 degree and AR=0.5. The effects of tail upwash on the surface pressure distribution of all wings were analyzed and the effects of wing sweep angle on the interaction were investigated. Tests were performed for both static and dynamic changes of the tail angle of attack at various fixed wing and body angles of attack.

2 Experimental Setup and Procedure

This section is divided into three subsections, namely: wind tunnel and test facility, model, and test procedures.

2.1 Wind Tunnel and Test Facility

Experiments were carried out in a subsonic closed circuit wind tunnel with a closed test section of $0.8 \times 0.8 \times 2$ m³. Figure 1 shows the wind tunnel and the test section. The maximum attainable speed in the test section is 100 m/s. Turbulence intensity of the wind tunnel is about 0.1%.

Surface pressure measurements were obtained by using differential transducers with ±1 and ±5 psi measuring limits. Prior to the tests, all transducers were carefully calibrated.
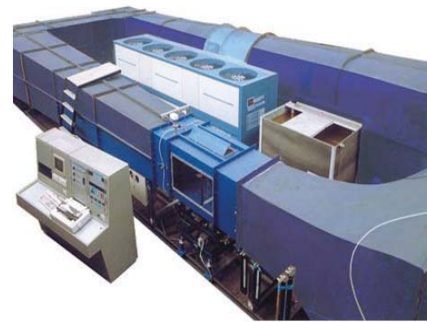

Figure 1. Wind tunnel and the test section.

2.2 Model

The model has three separate parts: body, wing and tail. The angle of attack of the body and the tail can be varied independently. Fig. 2 shows the model installed in the test section of the aforementioned wind tunnel.

Figure 2. Model in the wind tunnel test section.

Tests were conducted for two different wings with two different sweep angles: 30 and 60 degrees. Fig.3 presents different wings and tail geometry that were used in this investigation. 64 pressure sensors were applied to plot the wing surface pressure contour.
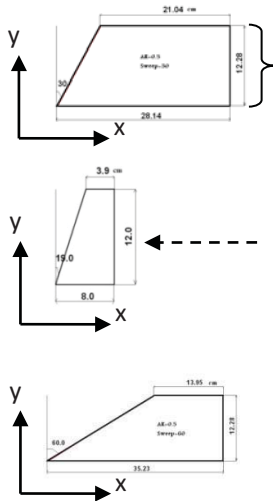
Figure 3. Wings and tail dimensions.

2.3 Test Procedures

Surface pressure, only upper surface, was measured at a free stream velocity of V=80 m/s corresponding to the Re=1.65×10^6, based on a wing root chord for all wings (As the vortex structure is independent of Reynolds number before the wing stall, this test can be used to understand the physics of vortex interactions at the original size model which may differ slightly from this Reynolds number) and the angles of attack of the wing were varied as α_w=10°, 15° and 20°. Several tests were performed for static and dynamic oscillation of the tail deflections. All tests were conducted on 2 different wings with sweep angles of 30° and 60°. An important parameter that was used in the results is the difference in the angle between the tail and the body-wing direction ($\Delta\alpha= \alpha_t - \alpha_w$). Fig. 4 represents this definition, $\Delta\alpha$, schematically.
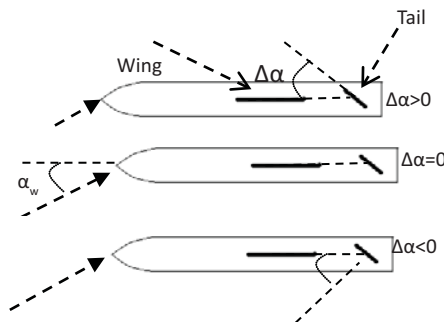
Figure 4. Definition of Δα.

A procedure similar to this was done for the dynamical changes of the tail A.O.A. The tail was oscillated with an oscillation frequency of ½ Hz and with oscillation amplitude of 5°. Surface pressure on the suction side of the wing was measured during all tests.

In order to account for the possible errors in the measured data, various data reduction schemes were applied to the raw data to reduce the effects of electrical and mechanical noises and other sources of errors.

3 Results and Discussion

This section is divided into two subsections, namely: wing with Λ_w=30° and wing with Λ_w=60°.

3.1 Wing with Λ_w=30°

Figure 5 shows the surface pressure contour for the wing with Λ_w=30° and at α_w=10°, α_w=15° and α_w=20° when $\Delta\alpha$=0. The structure of the leading edge vortex can be seen on the wing. Note that for this wing having a sweep angle of 30°, the flow field is not dominated by the vortices unlike delta wings with leading edge sweep of 60° and above. The flow over these wings is of vortex type ones. A small part of the wing is affected by the vortex like flow at α_w=10° and the leading edge vortex covers a large portion of the wing suction surface by increasing the A.O.A (α_w).

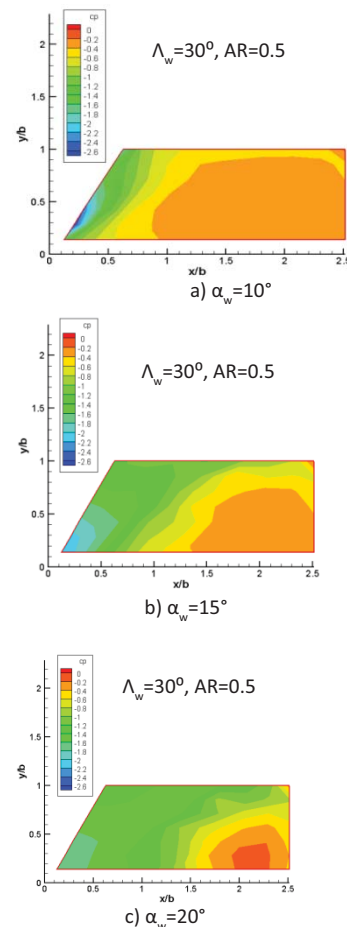a) α_w=10°

b) α_w=15°

c) α_w=20°

Figure 5. Contour of surface pressure coefficient on the 30° wing.

Figure 5a indicates that the maximum suction over the wing surface occurs around the leading edge, thus the zone near the leading edge plays an important role in the lift force produced by the wing. However, the power of the vortex on this zone decreases by increasing α_w. Wing surface pressure coefficients are compared with each other for all α_w's at two different wing sections, y/b=0.57, and at the leading edge of the wing in Fig. 6.
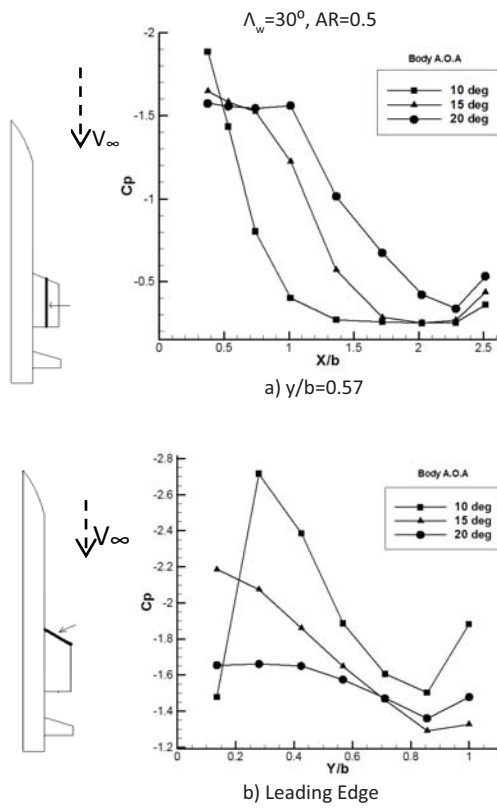
flow influences the strength and stability of the wing with $\Lambda_w=30^o$ when set to $\alpha_w=20^o$.

a) $\alpha_w=10°$

b) $\alpha_w=15°$

c) $\alpha_w=20°$
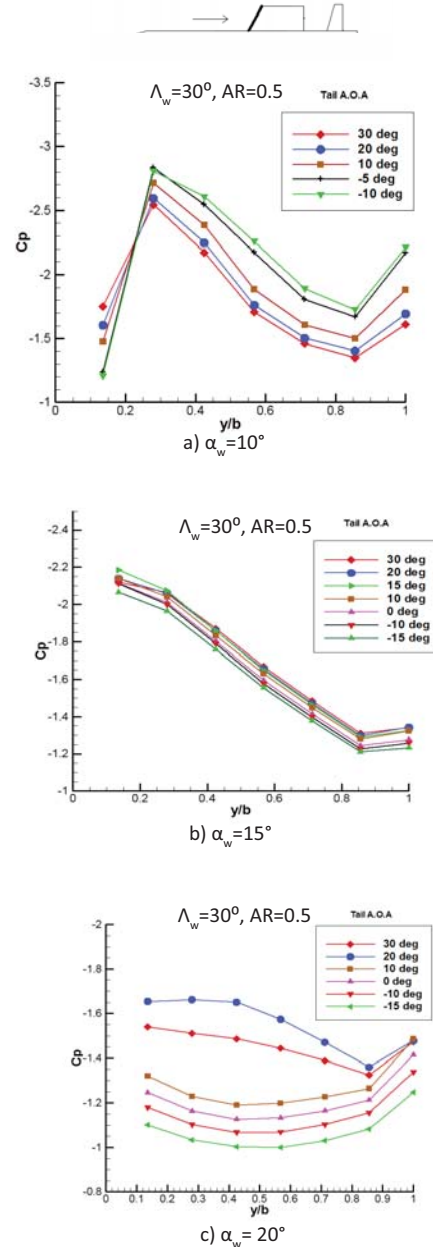
Figure 7. Cp at different α_t for the leading edge of the wing.

a) y/b=0.57

b) Leading Edge

Figure 6. Wing surface pressure coefficient.

From Fig. 6a, it is clearly seen that the vortex-like flow is developed on the wing's upper surface as α_w is increased. However, there exist some instabilities near the wing's leading edge at $\alpha_w=15^o$ and $\alpha_w=20^o$. Fig. 6b shows that the vortex strength at the wing's leading edge is weakened at $\alpha_w=15^o$ and $\alpha_w=20^o$. There exists a weak and unstable vortex on the wing's leading edge at $\alpha_w=20^o$. Fig. 6b shows that the vortex onset at $\alpha_w=10^o$ is not located at the apex of the wing.

Variations of Cp are shown for the wing's leading edge in Fig. 7 to study the case better. The vortex on the leading edge of the $\Lambda_w=30^o$ is weak and unstable at $\alpha_w=20^o$, Fig. 7c. Thus, any instability in the downstream

Figure 7c shows that the pressure distribution over the wing surface is highly influenced by the upwash of the tail at $\alpha_w=20^o$. The flow is very unstable at the wing's leading edge at $\alpha_w=20^o$ (Fig. 6b). Figure 7c indicates that, at $\Delta\alpha=0(\alpha_t=20^o)$ and $\Delta\alpha>0(\alpha_t=30)$, there exists pressure suction associated with the vortex-type flow over the wing's leading edge. However, the vortex

is completely diffused for $\Delta\alpha<0$. In Fig. 8, the reason for the aforementioned phenomenon is schematically shown.
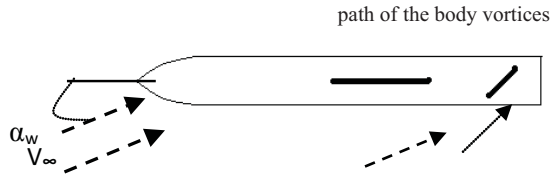
path of the body vortices

Figure 8. The path for body vortices.

This figure shows that at α_w=20° and for $\Delta\alpha<0$, vortices that are generated by the body merge with each other down stream of the wing through the path that tail makes. These vortices are very strong at α_w=20° and affect the formation of the vortex at the wing's leading edge.

Figure 9 shows the surface pressure contour at α_w=20° for both $\Delta\alpha$=0 (α_t=20°) and $\Delta\alpha$=-35° (α_t=-15°) for the wing with Λ_{LE}=30°. It is clearly seen that that instabilities associated with the body vortices at α_w=20°have influenced the wing surface pressure noticeably.

a) α_t=20°

b) α_t=-15°
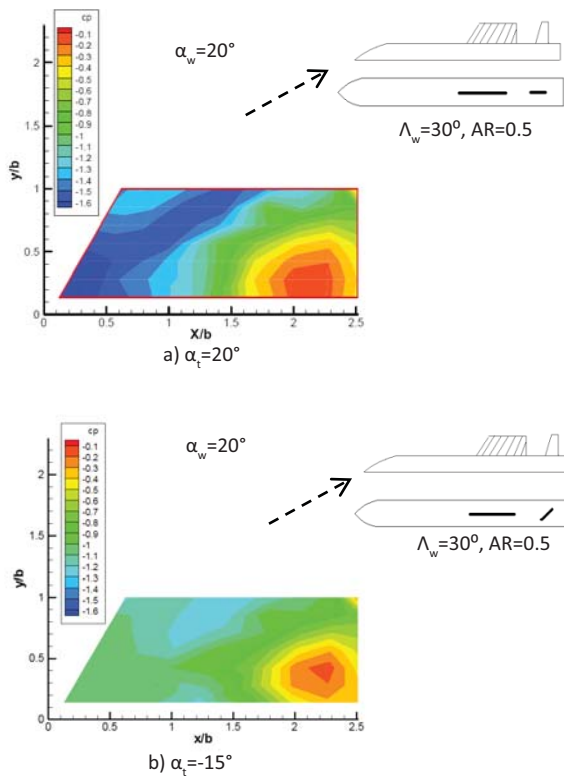
Figure 9. Effect of αt on the contours of surface pressure coefficient.

It is seen that $\Delta\alpha<0$ results in noticeable instabilities on the wing surface pressure but $\Delta\alpha>0$ has less effect on the pressure distribution. To investigate the physics of this phenomenon in depth, specially for $\Delta\alpha$=+10, a time history of Cp at the apex of the wing is presented in Fig. 10. From this Fig, it is seen that the strongest vortex is generated at α_t=20° or $\Delta\alpha$ =0° and there is no vortex structure at α_t=-15° or $\Delta\alpha$ =-35° as expected from our previous analysis. However, at α_t=30° or $\Delta\alpha$ =+10° the up wash related to the tail deflection has influenced the surface pressure near the leading edge of the wing in a different manner. There seems to be a delay in the onset of leading edge vortex formation at α_t=30° or $\Delta\alpha$ =+10°.
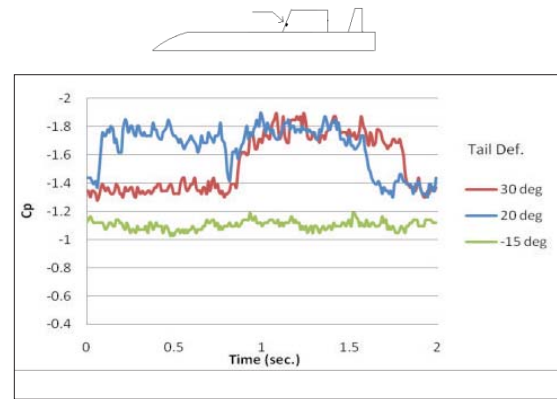
The power spectral density function of the Cp is ex-

Figure 10. Time history of C_p at the apex of the wing for α_w=20°.

tracted from the Cp time history for the pressure channel located at the apex of the wing. Variations of the PSD for different tail deflections are presented in Fig. 11. Investigation of the PSD plot indicates that the peaks of power spectral density of the surface pressure coefficient are detected for α_w=20°. Here, for α_w=20°, a main peak related to the leading edge vortex is generated at the frequency of about 2.5 Hz. At α_t=30° the vortex frequency is increased (a weaker peak of PSD is aligned with the frequency of 3.5 Hz). It seems that the generated vortex is slightly unstable at α_t=30°, ($\Delta\alpha$=+10°). Another point is that the vortex kinetic energy does not exist at different frequencies (unlike the case of α_t=20°). The reason for this phenomenon is the existence of the tail at the wing down stream that reduces the vortex core velocity for $\Delta\alpha>0$. The important point is that there exists no strong peak for α_t=-15°, Fig. 11. This may indicate that the kinetic energy of the leading edge vortex has been damped when the tail is set to α_t=-15°, ($\Delta\alpha$ =-35°).

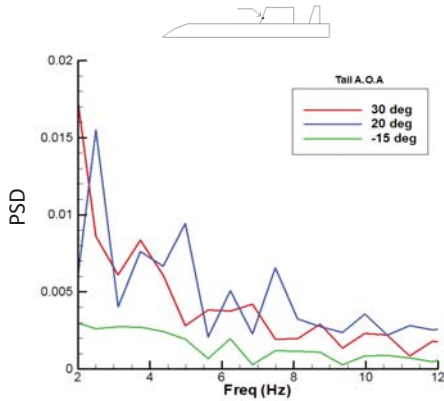**Figure 11. Frequency analysis at the apex of the wing for different Δα.**

Figure 12 shows the power spectral density of the pressure channels at the leading edge of the wing when the tail is oscillating with an oscillation frequency of 0.5 Hz and with an amplitude of 5° at α_w=15°.
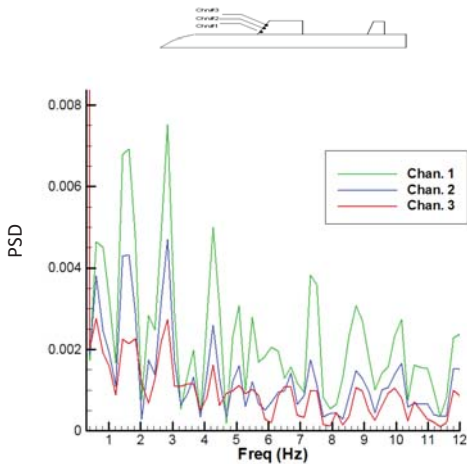

Figure 12. PSD of the pressure Channels at leading edge of the wing for oscillating tail.

There is a peak at a frequency of ½ Hz in Fig. 12 which shows the kinetic energy is induced to the vortex by the oscillating tail. Thus, the wing vortex is clearly affected by the tail upwash.

It is very important to know which parts of the wing suction are most affected by the oscillating tail upwash. The PSD values of all pressure channels for an oscillation frequency of ½ Hz are shown on the wing surface for α_w=15° in Fig. 13.
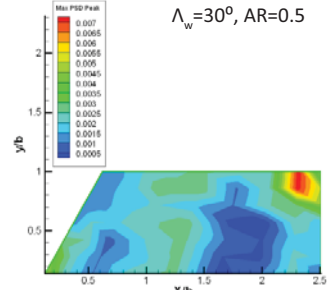
Figure 13. PSD values for all channels at α_w=20°, f=1/2 (Hz).

Comparing Fig. 13 with Fig. 5c, we realize that the influence of the tail upwash is at the place which is associated with the leading edge vortex on the wing. Furthermore, this figure clearly shows that the tail upwash affects almost the entire surface pressure over the wing surface when set to α_w=20°.

3.2 Wing with Λ_w=60°

Figure 14 shows the contour of the surface pressure coefficient over the wing with Λ_w=60° for α_w=10°, 15°, and 20° and at Δα=0. The structure of the leading edge vortex can be seen over the wing surface. A small part of the wing is affected by the vortex like flow at α_w=10° and the leading edge vortex covers a portion of the wing suction side by increasing A.O.A, α_w. The vortex strength and its stability increases by increasing the α_w, Fig.14.
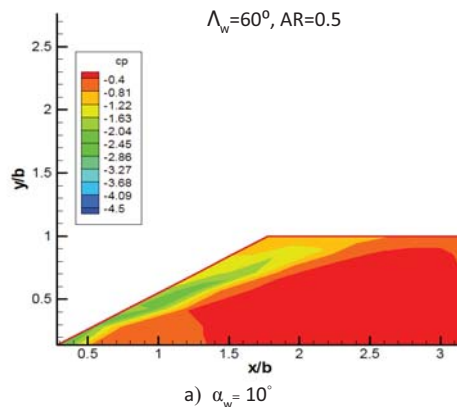

Figure 14. Contour of surface pressure coefficient on the 60° wing.
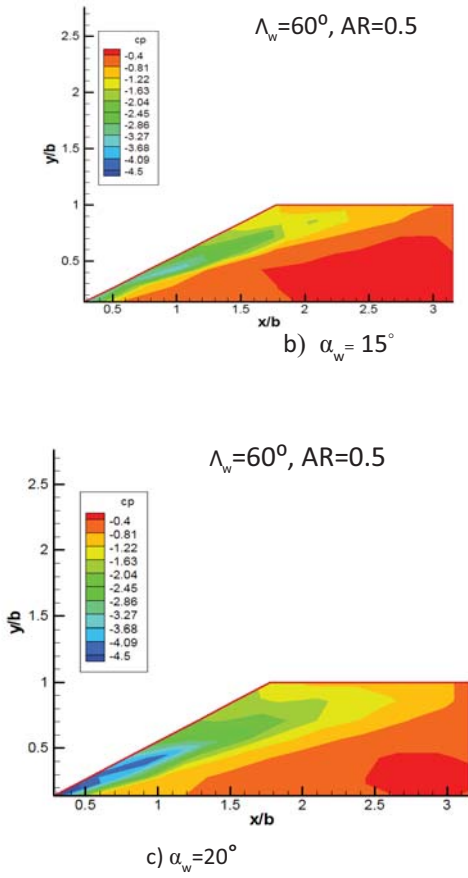
b) $\alpha_w = 15°$

c) $\alpha_w = 20°$

Figure 14. Cont'd.

Wing surface pressure coefficients are compared with each other for all αw's and for two different wing sections, i.e. y/b=0.57 and leading edge, in Fig. 15.
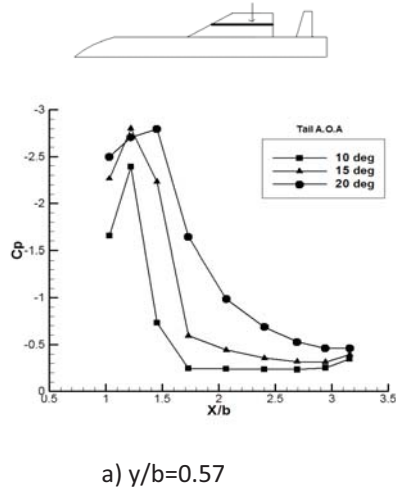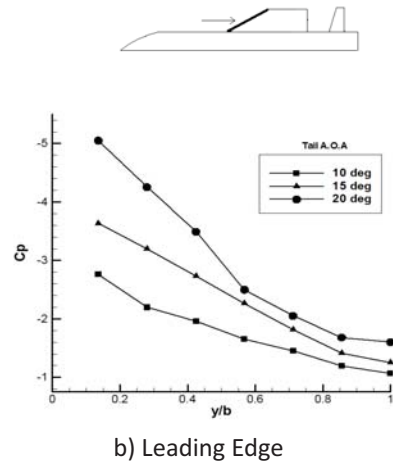

b) Leading Edge

Figure 15. Cont'd.

From Fig.15a, it is clearly seen that the vortex-like flow develops over the wing's upper surface as αw increases. The width of this region, low pressure, increases as the angle of attack is increased from $\alpha_w=10°$ to $\alpha_w=20°$. Fig. 15b shows that the suction strength of the vortex-type flow on the wing's leading edge also increases by increasing the αw. Thus, here the vortex at the leading edge of the wing is highly stable for these angles of attack, unlike the wing with $\Lambda_w=30°$, (Fig. 6b).

The effects of tail upwash on the wing surface pressure are shown in Fig's. 16-17. Figure 16 shows variations of the wing Cp at y/b=0.57 section of the wing associated with the static changes in the tail angle of attack for different α_w's.

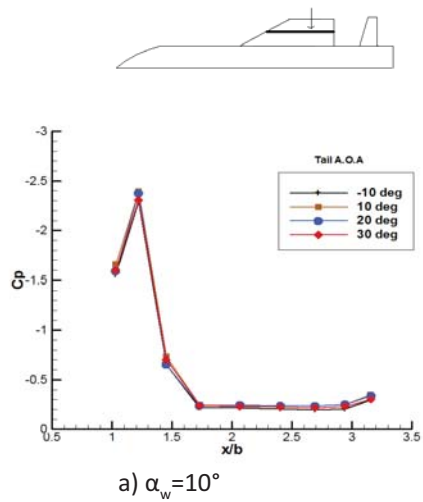a) y/b=0.57

Figure 15. Wing surface pressure coefficient.
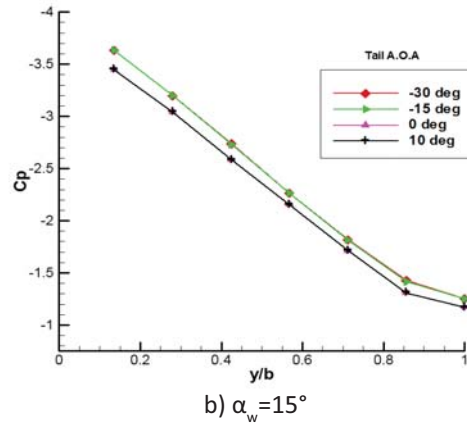

a) $\alpha_w=10°$

Figure 16. Cp at different α_t at y/b=0.57.

b) α_w=15°

c) α_w=20°

Figure 16. Cont'd.

b) α_w=15°

c) α_w=20°
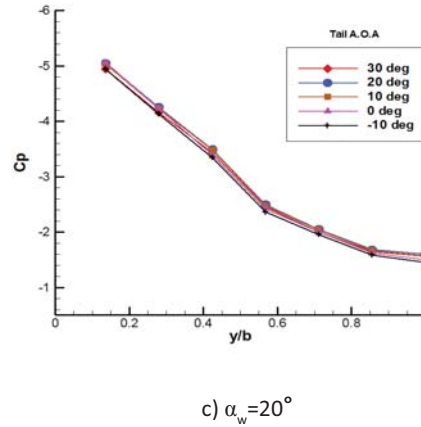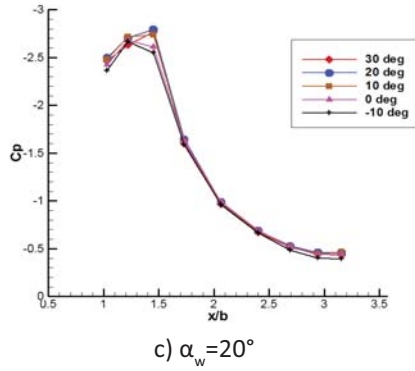
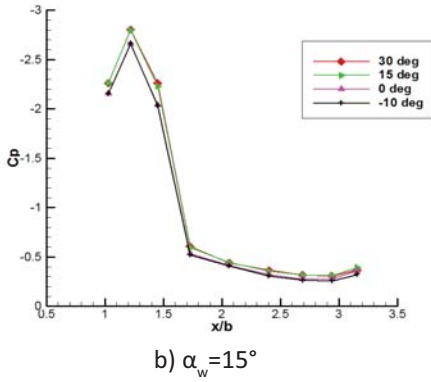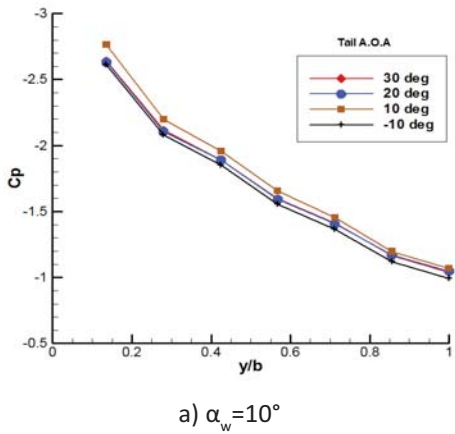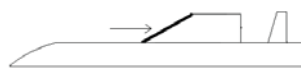**Figure 17. Cont'd.**

This figure indicates that the wing vortex is not affected by the tail upwash for the corresponding angles of attack of α_w=10°, α_w=15° and α_w=20°. To study the case better, variations of Cp are shown for the wing's leading edge in Figure 17.

a) α_w=10°

Figure 17. Cp at different α_t at leading edge.

This figure shows that a strong and stable vortex structure is generated on the wing's suction surface which is not influenced by the tail upwash easily. However, as seen from Figure 17b, for $\Delta\alpha$≥0, a jump in the Cp data for all y/b appears. Figure 18 shows time history of the Cp at the wing's leading edge for α_w=20° and for different α_t's. From this figure, it is seen that the tail deflection does not affect the apex for positive $\Delta\alpha$'s and for α_t=-10° ($\Delta\alpha$=-30°). However, when the tail angle is increased to α_t=-20° ($\Delta\alpha$=-40°), the |Cp| value reduces to almost zero, Figure 18, which may indicate that this tail setting has caused a complete flow separation over the wing surface all the way thru the wing apex. One may think of this tail setting as an aerodynamic break which will cause the lift to deteriorate completely.
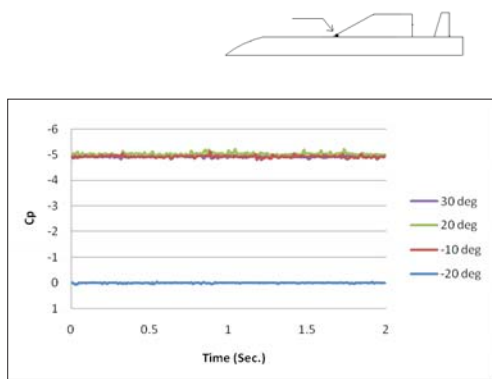
Figure 18. Time history of Cp at the apex of the wing for α_w=20º.

Figure 20. PSD of the pressure Channels at leading edge of the wing for oscillating tail.

Figure 19 shows the contour of the surface pressure over the 60º swept wing at α_w=20º and at $\Delta\alpha$=-40º. This figure indicates that the vortex structure is diffused over the entire wing surface at this tail deflection while, for $\Delta\alpha$=0, Fig's. 14-15 showed that a portion of wing surface is covered by the low pressure vortex-type flow.
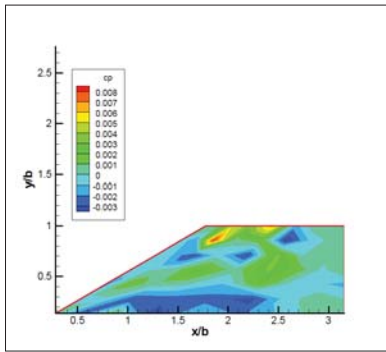
There is a peak at the frequency of 0.5 Hz in Fig. 20 which shows the kinetic energy induced to the vortex by oscillating the tail. Thus, the wing vortex is affected by the tail upwash. This figure indicates that the tail oscillation can even affect the highly stable vortex structure over the 60º wing.

It is very important to know which parts of the wing suction surface are affected the most by the oscillating tail upwash. The PSD values of all pressure channels for an oscillating frequency of ½Hz are shown in Fig. 21 for α_w=20º and for an amplitude of 5º.

Figure 19. Contour of surface pressure on the 60º wing at α_w=20º and ($\Delta\alpha$=-40º).

Figure 21. PSD values for all channels at α_w=20º, f=1/2 Hz.

Figure 20 shows the power spectral density of the pressure channel at the leading edge of the wing when the tail is oscillating with an oscillation frequency of ½Hz and with an amplitude of 5º at α_w=20º.

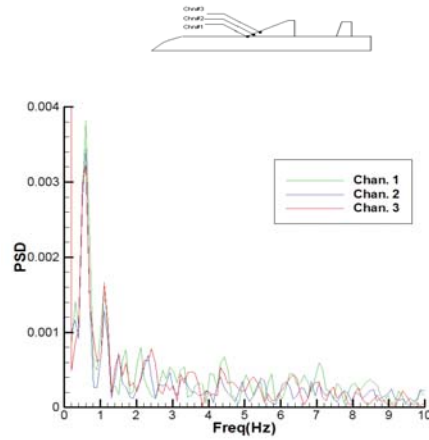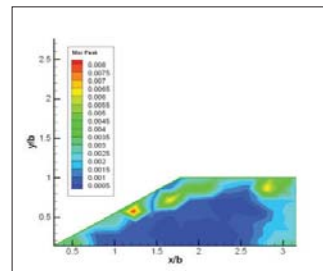It is seen from this figure that the Cp of the vortex onset at the apex of the wing is the most affected pressure channel. Comparing Fig. 21 with Fig.14c, we realize that the influence of the tail upwash is at the place which is associated with the leading edge vortex on the wing.

Figure 22 shows the PSD of the pressure channel located at the apex of the wing when the tail is oscillating with the frequency of ½Hz at different wing A.O.As. It is seen that the PSD value for the frequency of ½Hz, increases by increasing α_w.
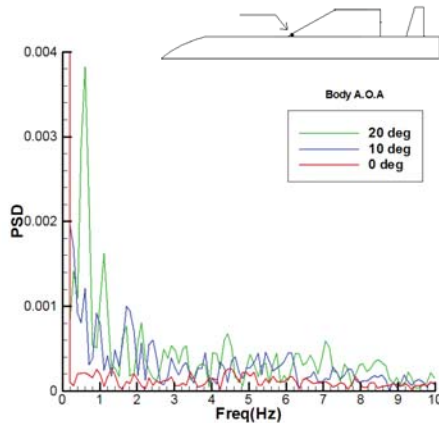
Figure 22. PSD value of the wing apex at different α_w for oscillating tail.

The reason for the aforementioned phenomenon is that the strength of body vortices increases by increasing α_w. Thus they cause more instability in the wing down stream flow.

Figure 23 shows the static surface pressure at the leading edge channels of wings with sweep angles of 30° and 60° at $\alpha w=20^o$ and for $\Delta\alpha=0$.
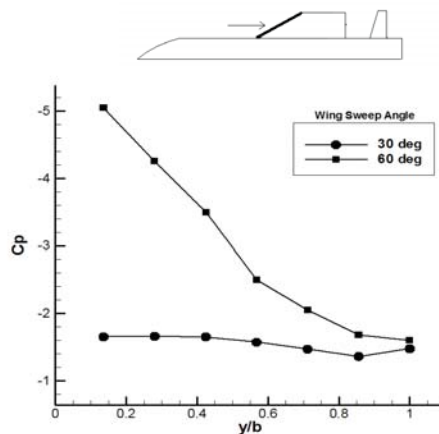

Figure 23. Surface pressure at the leading edge channels of all wings, $\alpha_w=20^o$ and $\Delta\alpha=0$.

This figure shows a strong vortex is formed on the suction surface of the 60° wing. The stability and strength of the vortex structure at this sweep angle leads to the low influence of the tail upwash on the surface static pressure on this wing.

4 Conclusion

A series of wind tunnel tests were performed to investigate the influence of tail deflection up wash on the leading edge vortex of two wings with different sweep angles in a body-wing-tail configuration. The Influence increases by increasing α_w. The reason for this phenomenon is that the vortices generated by the body merge with each other and make a strong instability at the wing down stream by increasing α_w. It was shown that this influence directly depends on the sweep angle of the wing. In other word, the vortex on the wing with 30 deg sweep angle is significantly affected by the up wash related to the tail deflection. For this wing the vortex on the wing is completely diffused at some tail deflections. For a wing with 60 deg sweep angle, there is no change on the leading edge vortex by the normal changes in the tail deflection. The reason for this phenomenon is due to the vortex strength and vortex stability. Note that the leading edge vortex strength and stability increases by increasing the wing sweep angle.

The quality of the leading edge vortex variations with static changes in the tail deflection directly depends on $\Delta\alpha$. The strongest and the most stable leading edge vortex is seen at $\Delta\alpha=0$ where body, wing and tail are at the same condition. Any change in $\Delta\alpha$ results in a weaker leading edge vortex formed over the wing surface. The effects of $\Delta\alpha>0$ and $\Delta\alpha<0$ are different. $\Delta\alpha<0$ makes more instabilities at the wing downstream.

The tail upwash due to the Oscillation affects the wing surface pressure more than the case for the static changes of the tail deflection. In this case the tail up wash affects the places on the wing surface where the vortex type flow is dominated. The most influenced pressure channel is the onset of the vortex at the wing apex for $\alpha_w=20^o$. The effects of oscillating tail up wash increases by increasing α_w.

5   References

1. Lesieutre, D.J., Dillenius, M.F.E., and Lesieutre, T.O., "Optimal Aerodynamic Design of Advanced Missile Configurations with Geometric and Structural Constraints", NEAR TR 520, Sep. 1997.

2. Lesieutre, D.J., Dillenius, M.F.E., and Lesieutre, T.O., "Missile Fin Planform Optimization for Improved Performance", Presented at NATO RTA/AVT Spring 1998 Symposium on Missile Aerodynamics, Paper 4, Sorrento, Italy, May 1998.

3. Lesieutre, D.J., Dillenius, M.F.E., Love, J.F., and Perkins, S.C., Jr., "Control of Hinge Moment by Tailoring Fin Structure and Planform", NEAR TR 530, Dec. 1997.

4. Lesieutre, D., Dillenius, M., and Lesieutre, T., "Multidisciplinary Design Optimization of Missile Configurations and Fin Planforms for Improved Performance", 7th Symposium on Multidisciplinary Analysis and Optimization, Sep. 1998.

5. Goswamia, R., Guptab, N.K., Ananthkrishnanc, N., Parkd, I.S., and Yoone, H.G., "Use of an Empirical Tool for Preliminary Aerodynamic Estimation of a Ducted Rocket Configuration", Aerospace Science and Technology, Nov. 27, 2009.

6. Blair, A.B. Jr., "Wind-Tunnel Investigation at Supersonic Speeds of a Canard-Controlled Missile With Fixed and Free-Rolling Tail Fins", NASA Technical Paper 1316, Sep. 1978.

7. Roshanian J. and Keshavarz Z., "Effect of Variable Selection on Multidisciplinary Design Optimization a Flight Vehicle Example", Chinese Journal of Aeronautics, Vol. 20, pp. 86-96, 2006.

8. Eric J. Abney and Melissa A. McDaniel, "High Angle of Attack Aerodynamic Predictions Using Missile Datcom", AIAA 2005-5086, June 2005.

9. Blair, A.B. , Jr., " Supersonic Aerodynamic Charactristics of a Maneuvering Canard – Controlled Missile with Fixed and Free-Rolling Tail Fins", SAE Paper 901993, Oct. 1990.

10. Nizam Dahalan Md., Su Vin Cent, and Shariff Ammoo Mohd., "Development of a Computer Program For Rocket Aerodynamic Coefficient Estimation" Journal Mekanika, No. 28, pp. 28- 43, June 2009.